Journal of Ceramic Processing Research. Vol. 21, Special. 1, pp. s53~s57 (2020)
(Received 17 December 2019, Received in revised form 24 March 2020, Accepted 2 April 2020)
https://doi.org/10.36410/jcpr.2020.21.S1.s53

JOURNAL OF
Ceramic Processing Research

Investigation of microstructural and electrical properties of self-aligned Ni-InGaAs alloy contacts to InGaAs as a function of rapid thermal annealing temperature

Shim-Hoon Yuk[a], Hyun-Gwon Park[a], V. Janardhanam[a], Kyu-Hwan Shim[a], Sung-Nam Lee[b] and Chel Jong Choi[a,*]
[a]*School of Semiconductor and Chemical Engineering, Semiconductor Physics Research Center (SPRC) Chonbuk National University, Jeonju 561-756, Republic of Korea*
[b]*Department of Nano-Optical Engineering, Korea Polytechnic University, Siheung 429-793, Republic of Korea*

We have investigated microstructural and electrical properties of self-aligned Ni-InGaAs alloy used as contact material to InGaAs as a function rapid thermal annealing (RTA) temperature. The Ni-InGaAs alloy was the only phase resulting from solid-state reaction between Ni and InGaAs, regardless of the RTA temperature. Microstructural evolutions of Ni-InGaAs and overlaid Ni films were observed for increasing RTA temperature. The increase in RTA temperature resulted in increasing the size of the pinholes formed in the Ni film, which could be associated with the columnar growth nature of sputter-deposited Ni film. A relatively uniform Ni-InGaAs layer was formed after RTA at 300 °C, which could be responsible for the minimum specific contact resistivity observed at this temperature. Above this temperature, the Ni-InGaAs layer underwent severe structural degradation such as the formation of microvoids in its surface area, leading to a rapid increase in specific contact resistivity.

Keywords: InGaAs, Ni, Specific contact resistivity, RTA, Solid-state reaction.

Introduction

InGaAs has attracted much interest as a channel material for metal-oxide-semiconductor field-effect transistors (MOSFETs) because of its high electron mobility and light electron effective mass. To realize excellent performance and highly reliable operation of InGaAs channel MOSFETs, their source/drain (S/D) contact resistance should be minimized. A general approach to reduce the S/D contact resistance is by doping the S/D regions heavily enough that the tunneling of carriers through S/D contact is possible. Namely, an increase in doping concentration of S/D regions leads to the significant reduction of S/D contact resistance. However, because of the low dopant solubility in InGaAs, the typical reduction of S/D contact resistance through an increase of the doping concentration is limited [1]. To overcome this problem, a reliable, and low-resistance Ohmic contact between the S/D and InGaAs is essential [2-4]. There have been many reports of non-alloyed, Ti-based Ohmic contacts to InGaAs, with specific contact resistivity of $\sim 2 \times 10^{-7}$ Ω×cm^2 [5-8]. Additionally, TiW-, Mo-, Pd-, WSi-, and ErAs-based materials have been proposed as alternatives for contacting InGaAs [9-15].

Similar to self-aligned silicides or germanides, which are formed by depositing a metal film on Si or Ge and combined with thermal treatment at elevated temperature, the metal-InGaAs alloys formed in a self-aligned manner through a solid-state reaction between a metal and InGaAs are highly required, in particular for deeply scaled InGaAs-channel MOSFETs [1, 16]. Among various metals, Ni has been considered as a viable candidate for self-aligned alloy formation, which is feasible for providing a low-resistance Ohmic contact to InGaAs for the realization of ultra-low power devices [17, 18]. At present, considerable efforts have been made to characterize Ni-InGaAs alloys formed by solid-state reaction between Ni and InGaAs driven by thermal treatment and demonstrate its potential use as self-aligned Ohmic contact in devices. Kim et al. [1] reported for the first time that, in InGaAs MOSFETs fabricated by forming self-aligned Ni–InGaAs alloy S/D formed at 250 °C and engineering the Schottky barrier, the S/D resistance was 1/5 lower than in p–n junction devices. Similarly, it was shown that using self-aligned Ni-InGaAs contacts, formed by sputtering a Ni film on single-crystalline InGaAs followed by low-temperature annealing in the 250–400 °C range, was feasible to realize the n-type MOSFETs with on-/off-state drain current ratio of $\sim 10^3$ [19]. A different study reported that surface passivation of InGaAs through an InP capping layer or a $(NH_4)_2S$ surface treatment reduced the Ni-InGaAs/InGaAs contact resistivity effectively [20]. Eadi et al. [21] demonstrated that the specific contact resistivity of Ni-InGaAs/InGaAs was lower in presence of the Tm interlayer than in its absence. This could be caused by uniform distribution and pile-up of

*Corresponding author:
Tel : +82-63-270-3365
Fax: +82-63-270-3585
E-mail: cjchoi@jbnu.ac.kr

Si dopant atoms near the Ni-InGaAs/InGaAs interface after introducing the Tm interlayer. However, most previous works have concentrated mainly on process techniques to minimize the specific contact resistivity of Ni-InGaAs/InGaAs contacts for realizing high performance devices. The dependence of the detailed Ohmic contact on the microstructural features of the Ni-InGaAs alloy is of great importance for the successful process integration of self-aligned S/D Ohmic contacts into InGaAs-based MOSFETs. Nevertheless, the reports on the relation between electrical and microstructural properties of the Ni-InGaAs/InGaAs contact formed by solid-state reaction between Ni and InGaAs driven by thermal treatment are limited. In this work, we investigated the microstructural and electrical properties of self-aligned Ni-InGaAs alloy/InGaAs contact formed through Ni deposition followed by rapid thermal annealing (RTA) process as a function of the RTA temperature. In particular, the variation of the Ni-InGaAs/InGaAs specific contact resistivity depending on RTA temperature is directly correlated with the microstructural evolution of the Ni-InGaAs and overlaid unreactive Ni layers during the RTA process.

Experimental Details

In this study, a 20 nm-thick $In_{0.53}Ga_{0.47}As$ (InGaAs) epilayer with a doping concentration of 5 ´ 10^{19} cm^3 grown on an InP substrate and an InAlAs buffer layer were used, which was manufactured by IntelliEPI, Inc. From Hall measurements, the carrier concentration of InGaAs epilayer was found to be 1.9×10^{19} cm^3, of which value was comparable to that provided by the manufacturer. Prior to Ni deposition, the sample was chemically cleaned for 10 min in acetone and methanol and rinsed in de-ionized water to remove contaminants from the surface of the substrate. Then, the sample was treated with a diluted HF solution to remove the native oxide. A Ni film with thickness 50 nm was sputter-deposited on the clean InGaAs epilayer in vacuum, at a pressure of 1×10^{6} Torr. Finally, RTA process was performed at temperatures in the range of 200–400 °C for 1 min under N_2 ambient for a solid-state reaction between Ni and InGaAs. When considering the limitation of enhancing Ohmic properties through the increase in the doping concentration associated with the low dopant solubility in InGaAs, all contacts were formed on InGaAs epilayer with a fixed doping concentration of 5×10^{19} cm^3. To extract the specific contact resistivity, circular transmission line method (CTLM) patterns with a constant inner radius of 200 mm and the inner/outer radius gaps varying from 5 to 50 mm were defined using standard photolithography. The current–voltage (I–V) characteristics of the Ni contacts to the InGaAs epilayer were measured before and after RTA using the precision semiconductor parameter analyzer (Agilent 4156C). The phase evolution of the samples, driven by the RTA process, was identified using high-resolution X-ray diffraction (HR-XRD, PANalytical X'Pert Pro MRD). The microstructures of the samples were characterized by field-emission transmission electron microscope (FETEM, FEI Tecnai F30). The surface morphology and root-mean-square (RMS) roughness of the samples were characterized by field-emission scanning electron microscopy (FESEM, S4200, Hitachi Ltd.) and atomic force microscopy (AFM, n-Tracer, NanoFocus Inc.), respectively.

Results and Discussion

Fig. 1 shows the HR-XRD plots of the Ni contacts to the InGaAs epilayer as a function of RTA temperatures in the 200–400 °C range. All samples exhibited the XRD peak with highest diffraction intensity at 63.4°, corresponding to the InP substrate. Since the InGaAs epilayer and InAlAs buffer layer are lattice-matched to the InP substrate, with the same crystal structure, their XRD peaks overlap with the strong InP substrate peak [22]. In fact, these could not be sharply separated in XRD spectra because of very similar XRD peak positions. In addition to the XRD peaks related to the InP substrate, the characteristic Ni(111) peak was clearly observed for the as-deposited and 200 °C-annealed samples. However, for annealing temperatures above 300 °C, an additional peak corresponding to the Ni-InGaAs formed by solid-state reaction of Ni and InGaAs was visible. A similar RTA temperature-dependent phase evolution of the Ni/InGaAs contacts was observed by Kim et al. [1]. They reported that Ni–InGaAs alloy formed after annealing at temperatures between 250 and 450 °C. Additionally, the presence of the Ni(111) peak in the samples annealed at 300 and 400 °C indicates that, in thermal treatments above 300 °C, not the whole deposited Ni film reacted with the underlying InGaAs epilayer.

Fig. 2 exhibits the scanning transmission electron microscopy (STEM) Z-contrast images taken from the Ni contacts to the InGaAs epilayer treated by RTA in

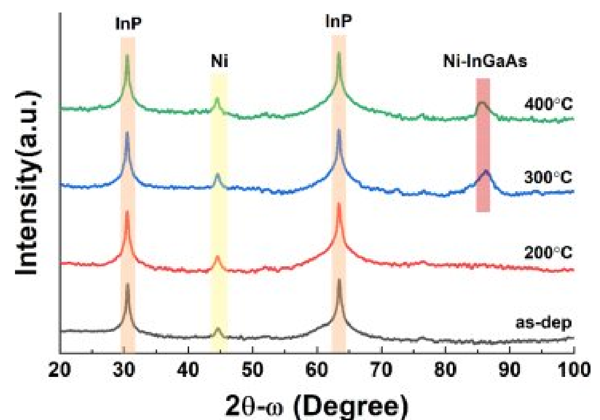

Fig. 1. HR-XRD plots of the Ni contacts to InGaAs epilayers as a function of RTA temperatures in the range of 200–400 °C.

the 200–400 °C temperature range. It is clear that the columnar growth structure of Ni films, with grain boundaries oriented perpendicular to the substrate surface irrespective of the annealing temperature. Such a columnar growth is a typical feature of sputter-deposited Ni films associated with rotational mismatch between adjacent Ni grains around the [110] axis [23]. The increase of the RTA temperature resulted in evolution of the pinholes formed between columnar Ni grains, *i.e.*, the size of the pinholes increased for increasing RTA temperatures. As seen in Fig. 2(a) for a sample annealed at 200 °C, a layer with a bright contrast was observed in-between Ni and the InGaAs epilayer. This layer is believed to be Ni-InGaAs alloy formed by Ni/InGaAs reaction during the RTA process. The Ni-InGaAs layer formed after RTA at 200 °C was irregular, with the thickness of ~ 4 nm. This implies that RTA at 200 °C is not sufficient to induce solid-state interfacial reaction between the Ni film and the InGaAs epilayer. However, the presence of the very thin, non-uniform Ni-InGaAs layer was not detected in the HR-XRD measurements (Fig. 1). As seen from these, the samples annealed at 300 and 400 °C displayed clearly the Ni-InGaAs layer formed by Ni/InGaAs reaction driven by RTA process along with the unreacted Ni film. The RTA process at 300 °C yielded the formation of a Ni-InGaAs layer with a relatively uniform surface and interface morphology. An unreacted InGaAs epilayer was found after solid-state reaction between Ni and InGaAs induced by RTA at 300 °C. On the other hand, this epilayer was not observed in the sample annealed at 400 °C. In other words, the InGaAs epilayer was fully consumed by Ni during Ni/InGaAs reaction at this temperature. There was no further reaction between Ni and InAlAs, resulting in a very abrupt interface between Ni-InGaAs and InAlAs. Furthermore, after RTA process at 400 °C, agglomeration or phase separation of Ni-InGaAs, causing the disintegration of film continuity, was not observed. However, a structural degradation of the Ni-InGaAs film was observed, and related to the formation of the microvoids indicated by arrows in Fig. 2(c). In general, the solid-state reaction between films involves the process of in/out-diffusion for the formation of the alloys. It is exactly not clear about the in diffusion of Ni or the out diffusion of elements in InGaAs for the formation of the Ni-InGaAs alloy at this moment. However, when considering the formation of microvoids shown in Fig. 2(c), the massive out-diffusion of elements consisting of InGaAs might be predominant for the formation of Ni-InGaAs alloy at higher temperature.

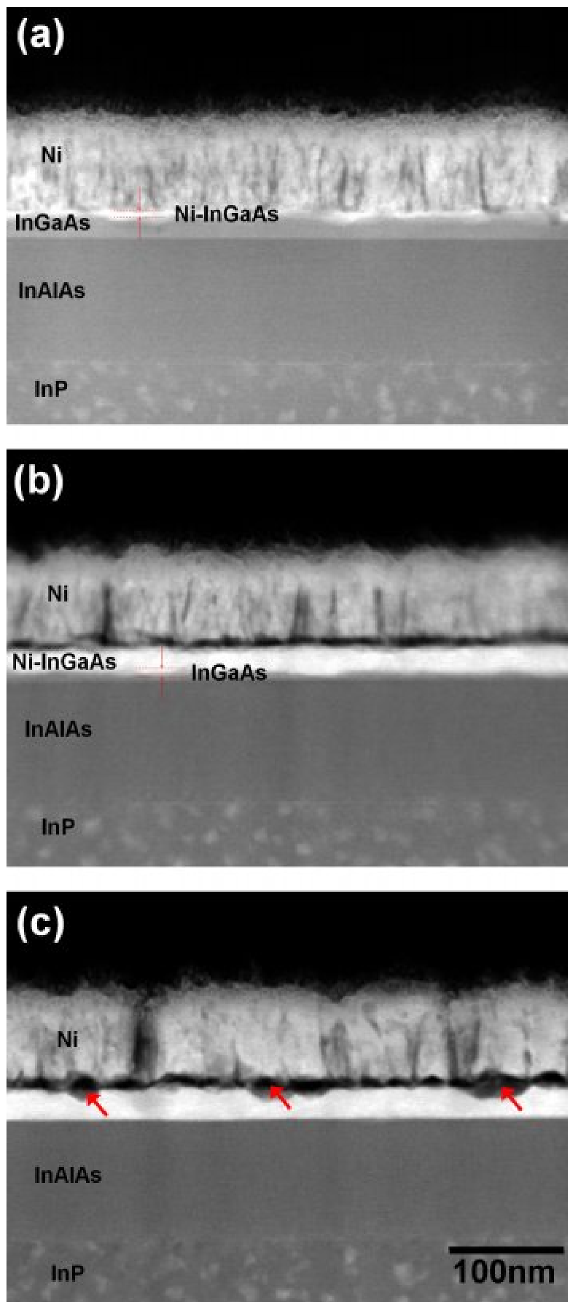

Fig. 2. STEM Z-contrast images of the Ni contacts to InGaAs epilayers treated by RTA at (a) 200 °C, (b) 300 °C, and (c) 400 °C.

Fig. 3 displays plan-view SEM images of the Ni contacts to the InGaAs epilayers after annealing at 200, 300, and 400 °C. The images clearly show an evolution of the surface morphology of Ni films as the RTA temperature increases. The surface of the sample annealed at 200 °C was smooth and featureless. The value of the corresponding RMS roughness, extracted from AFM measurements (not shown here), was found to be 1.10 nm. In the sample annealed at 300 °C shown in Fig. 3(b), the surface roughened slightly, displaying the very tiny pinholes indicated by arrows in the figure, and the RMS roughness increased to 1.29 nm. In the sample annealed at 400 °C, severe morphological degradation of the surface was observed, as seen from Fig. 3(c). Namely, numerous large-scale pinholes were randomly distributed on the surface after RTA process at 400 °C, which were in a good agreement with TEM results (Fig. 2). Additionally, the energy-dispersive X-ray spectroscopy (EDS) analyses (not shown here) did not reveal differences

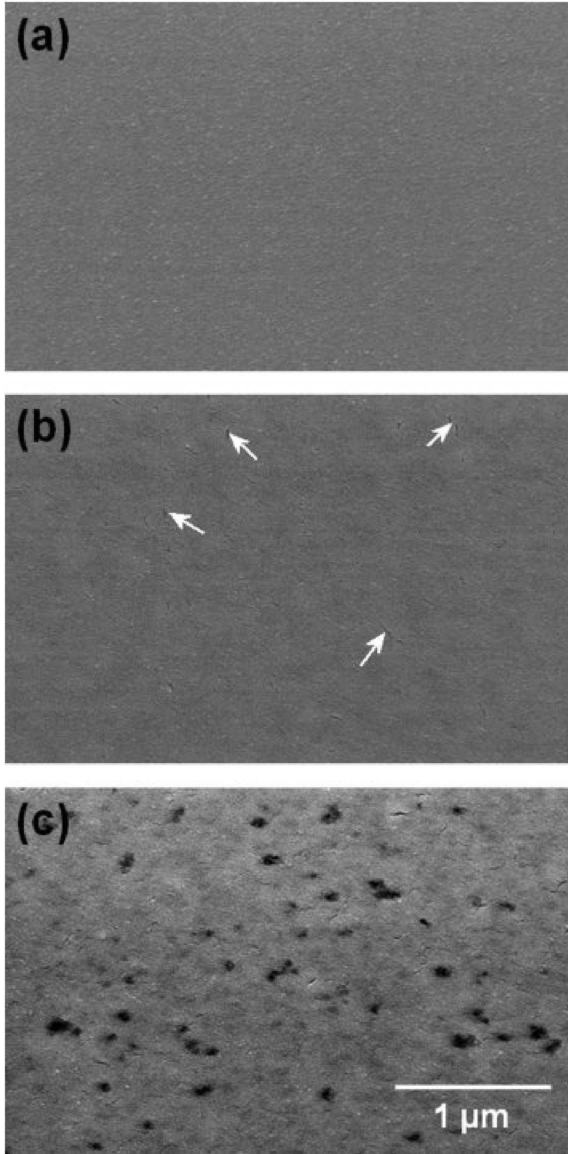

Fig. 3. Plan-view SEM images of the Ni contacts to the InGaAs epilayers treated by RTA at (a) 200 ºC, (b) 300 ºC, and (c) 400 ºC.

among the sample. This could be attributed in part to the presence of unreactive Ni film on surface shown in Fig. 2 and to the large specimen interaction volume caused by accelerated electron beam.

Fig. 4 shows the plot of the specific contact resistivity of Ni contacts to InGaAs epilayers as a function of RTA temperature. In particular, four-terminal CTLM measurements were carried out to avoid the parasitic resistance associated with measurement setup used for measuring the specific contact resistivity, as shown in the inset of Fig. 4. The specific contact resistivity was extracted from the CTLM method using following equations [24]

$$R_T = R_{sh}(S + 2L_T)C \tag{1}$$

$$C = \frac{r}{s}\ln\left(1 + \frac{s}{r}\right) \tag{2}$$

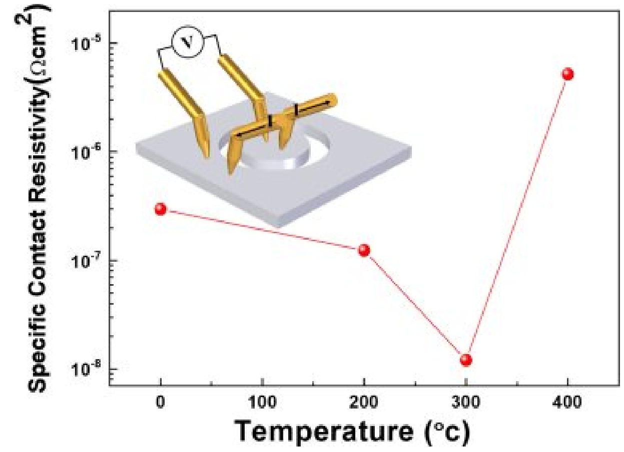

Fig. 4. Plot of the specific contact resistivity of the Ni contacts to the InGaAs epilayers as a function of RTA temperature. The Inset shows measurement setup used for measuring the specific contact resistivity through four-terminal CTLM measurements.

$$\rho_c = R_{sh}L_T^2 \tag{3}$$

where, R_{sh} is the sheet resistance, C is the correction factor, L_T is the effective transfer length, r is the radius of the inner circle, which was fixed at 200 µm, and s is the gap space, which was split as 5, 10, 15, 25, 35 and 50 µm. A specific contact resistivity r_c is calculated using R_{sh} and L_T values determined from a linear fit of R_T at the different gap space values. The specific contact resistivity of 2.97×10^{-7} W×cm^2 was obtained for the as-deposited sample. The RTA process at 200 ºC led to a slight decrease in specific contact resistivity to 1.23×10^{-7} W×cm^2. This could be attributed to the formation of the thin Ni-InGaAs layer shown in Fig. 2(a). In other words, the solid-state reaction between Ni and the InGaAs epilayer allows the effective removal of the surface damage caused by the exposure of plasma during sputter-deposition of Ni or the contamination on surface of the InGaAs epilayer that was unintentionally introduced during the fabrication process, which can serve as a major cause of the increase in the specific contact resistivity. A specific contact resistivity further reduced to 1.02×10^{-8} W×cm^2 was found after RTA at 300 ºC. Such a low value could be associated with the formation of a fairly uniform Ni-InGaAs layer. It should be noted that the specific contact resistivity obtained after RTA at 300 ºC is lower than those reported for the Ni-InGaAs contact to InGaAs [21, 25, 26]. This implies that Ohmic contact process is feasible for the successful implementation of high performance InGaAs channel MOSFFETs. However, a steep increase in the specific contact resistivity was observed after RTA at 400 ºC. As shown by the TEM image of Fig. 3(c), a Ni-InGaAs layer with uniform interface and surface morphologies was formed after RTA at 300 ºC. Above this temperature, the morphologies of Ni-InGaAs and of the overlaying unreactive Ni films were significantly degraded, *i.e.*, the formation of microvoids

and pinholes in the former and the latter, respectively. Namely, the severe structural degradation of both the Ni-InGaAs and Ni films during RTA at 400 °C could be the main cause of the large increase in specific contact resistivity.

Conclusions

Self-aligned Ni-InGaAs Ohmic contacts on an InGaAs epilayer were formed by sputter-deposition of a Ni film followed by subsequent RTA process at temperatures in the 200–400 °C range. The variation of the specific contact resistivity of the Ni-InGaAs contact to InGaAs caused by RTA process was explained in terms of the microstructural evolutions of the Ni-InGaAs layer and overlaid unreactive Ni layer. Although an irregular Ni-InGaAs layer formed after RTA at 200 °C, the sample annealed at this temperature showed a specific contact resistivity slightly lower than the as-deposited one. This could be associated with the curing of plasma damage or unintentional film contamination through the solid-state reaction between Ni and InGaAs driven by RTA process at 200 °C. A fairly uniform Ni-InGaAs layer was formed as a result of Ni/InGaAs solid-state reaction after RTA at 300 °C, which could be responsible for the minimum specific contact resistivity measured at this temperature. However, RTA at 400 °C led to the formation of microvoids on the surface of the Ni-InGaAs layer and the presence of a sizable number of pinholes in the overlaying unreactive Ni film. Such a structural degradation could be the main cause of a larger increase in specific contact resistivity. The results obtained here demonstrate that the Ni-InGaAs alloy formed by the self-aligned process could be a promising S/D contact material for the minimization of specific contact resistivity. Furthermore, the RTA temperature-dependency of the specific contact resistivity of Ni-InGaAs contact to InGaAs reported in this work provides a valuable process guideline for realizing the high performance InGaAs channel MOSFETs.

Acknowledgements

This study was supported by the National Research Foundation of Korea (NRF) Grant (NRF-2017R1A2B 2003365) funded by the Ministry of Education, Republic of Korea, and by Korea Evaluation Institute of Industrial Technology (KEIT) grant (Project No. 20004314) funded by the Ministry of Trade, Industry & Energy, Republic of Korea.

References

1. S.H. Kim, M. Yokoyama , N. Taoka , R. Iida , S. Lee, R. Nakane, Y. Urabe, N. Miyata, T. Yasuda, H. Yamada, N. Fukuhara, M. Hata, M. Takenaka, and S. Takagi, Appl. Phys. Exp. 4 (2011) 024201.
2. S. Takagi, T. Tezuka, T. Irisawa, S. Nakaharai, T. Numata, K. Usuda, N. Sugiyama, M. Shichijo, R. Nakane, and S. Sugahara, Solid-State Electron. 51 (2007) 526-536.
3. X. Li, R. J. W. Hill, P. Longo, M. C. Holland, H. Zhou, S. Tohms, D. S. Macintyre, and I.G. Thayne, J. Vac. Sci. Technol. B 27 (2009) 3153-3157.
4. M. Yokoyama, T. Yasuda, H. Takagi, H. Yamada, N. Fukuhara, M. Hata, M. Sugiyama, Y. Nakano, M. Takenaka, and S. Takagi,Dig. Tech. Pap. - Symp. VLSI Technol. (2009) 242-243.
5. D. Caffin, C. Besombes, J. F. Bresse, P. Legay, G. L. Roux, G. Patriarche, and P. Launay, J. Vac. Sci. Technol. B 15, 854 (1997).
6. E. Nebauer, M. Mai, E. Richter, and J. Wurfl, J. Electron. Mater. 27, 1372 (1998).
7. J. Wu, C. Chang, K. Lin, E. Chang, J. Chen, and C. Lee, J. Electron. Mater. 24, 79 (1995).
8. T. Nittono, H. Ito, O. Nakajima, and T. Ishibashi, Jpn. J. Appl. Phys. 27, 1718 (1988).
9. A. M. Crook, E. Lind, Z. Griffith, M. J. W. Rodwell, J. D. Zimmerman, A. C. Gossard, and S. R. Bank, Appl. Phys. Lett. 91, 192114 (2007).
10. A. K. Baraskar, M. A. Wistey, V. Jain, U. Singisetti, G. Burek, B. J. Thibeault, Y. J. Lee, A. C. Gossard, and M. J. W. Rodwell, J. Vac. Sci. Technol. B 27, 2036 (2009).
11. A. Baraskar, M. A. Wistey, V. Jain, E. Lobisser, U. Singisetti, G. Burek, Y. J. Lee, B. Thibeault, A. Gossard, and M. Rodwell, J. Vac. Sci. Technol. B 28, C5I7 (2010).
12. A. S. Wakita, N. Moll, S. J. Rosner, and A. Fischer-Colbrie, J. Vac. Sci. Technol. B 13, 2092 (1995).
13. E. F. Chor, W. K. Chong, and C. H. Heng, J. Appl. Phys. 84, 2977 (1998).
14. N. Yoshida, Y. Yamamoto, H. Takano, T. Sonoda, S. Takamiya, and S. Mitsui, Jpn. J. Appl. Phys. 33, 3373 (1994).
15. U. Singisetti, J. D. Zimmerman, M. A. Wistey, J. Cagnon, B. J. Thibeault, M. J. W. Rodwell, A. C. Gossard, S. Stemmer, and S. R. Bank, Appl. Phys. Lett. 94, 083505 (2009).
16. X. Zhang, H.Guo, X. Gong, Q. Zhou,Y.-R.Lin,H.-Y.Lin, C.-H.Ko, C. H. Wann, and Y.-C. Yeo, Electrochem. Solid-State Lett. 14 (2011) H60-H62.
17. Ivana, Y.L. Foo, X. Zhang, Q. Zhou, J. Pan, E. Kong, M.H.S. Owen, and Y.-C. Yeo, J. Vacuum Sci. Technol. B 31 (2013) 012202.
18. P. Shekhter, S. Mehari, D. Ritter, and M. Eizenberg, J. Vacuum Sci. Technol. B 31 (2013) 031205.
19. X. Zhang, Ivana, H.X. Guo, X. Gong, Q. Zhou, and Y.-C. Yeo, J. Electrochem. Soc. 159 (2012) H511-H515.
20. M. Abraham, S.-Y. Yu, W. H. Choi, R.T.P. Lee, and S.E. Mohney, J. Appl. Phys. 116 (2014) 164506.
21. S.B. Eadi, J.C. Lee, H.-S. Song, J. Oh, and H.-D. Lee, Vacuum 166 (2019) 151-154.
22. S. Mehari, A. Gavrilov, S. Cohen, P. Shekhter, M. Eizenberg, and D. Ritter, Appl. Phys. Lett. 101 (2012) 072103.
23. J. W. Patten, Thin Solid Films 75 (1981) 205-211
24. S. B. Eadi, J. C. Lee, H. S. Song, J. O, and H. D. Lee, Vacuum 166 (2019) 151-154
25. S. Kim, S.K. Kim, S. Shin, J._H. Han, D.M. Geum, J.-P. Shim, S. Lee, H. Kim, G. Ju, J.D. Song, M.A. Alam, H.-J. Kim, J. Electron Devices Soc. 7 (2019) 869-877.
26. X. Zhang, H.X. Guo, X. Gong, Y.-C. Yeo, ECS J. Solid State Sci. Technol. 1 (2012) P82-P85.